E15-2009-177

O. Svoboda[1,2,*], J. Adam[1,3], M. Bielewicz[4], I. Hartwing[1,5], S. Kilim[4], A. Krása[1], M. I. Krivopustov[3], A. Kugler[1], M. Majerle[1,2], E. Strugalska-Gola[4], M. Szuta[4], V. M. Tsoupko-Sitnikov[3], V. Wagner[1,2], W. Westmeier[6], A. Wojciechowski[4], I. Zhuk[7]

STUDY OF SPALLATION REACTIONS, NEUTRON PRODUCTION AND TRANSPORT IN THICK LEAD TARGET AND URANIUM BLANKET IRRADIATED WITH 0.7 GeV PROTONS

Submitted to «Nuclear Instruments and Methods in Physics Research A»

[1]Nuclear Physics Institute of the Academy of Sciences of the Czech Republic, Řež, the Czech Republic
[2]Faculty of Nuclear Sciences and Physical Engineering, Czech Technical University, Prague, the Czech Republic
[3]Joint Institute for Nuclear Research, Dubna, Russia
[4]Institute of Atomic Energy, Otwock-Świerk, Poland
[5]Technische Universität Chemnitz, Chemnitz, Germany
[6]Philipps-Universität, Marburg, Germany
[7]Joint Institute of Power and Nuclear Research, Sosny, Minsk, Belarus
[*]E-mail: svoboda@ujf.cas.cz

Свобода О. и др. E15-2009-177

Изучение реакций глубокого расщепления, образования
и прохождения нейтронов в толстой свинцовой мишени
и урановом бланкете под действием протонов с энергией 0,7 ГэВ

Нейтронно-активационные детекторы использовались для исследования нейтронного поля в установке «Энергия плюс трансмутация», состоящей из толстой свинцовой мишени и бланкета из натурального урана. Установка облучалась протонами с энергией 0,7 ГэВ от сверхпроводящего ускорителя нуклотрон. Эксперимент был этапом в систематических исследованиях с использованием протонных и дейтериевых пучков в интервале энергий от 0,7 до 2,52 ГэВ. Экспериментальные данные сравнивались с расчетами MCNPX и данными других экспериментов. Наблюдалось хорошее согласие в пределах статистических и систематических неопределенностей.

Работа выполнена в Лаборатории ядерных проблем им. В. П. Джелепова ОИЯИ.

Препринт Объединенного института ядерных исследований. Дубна, 2009

Svoboda O. et al. E15-2009-177

Study of Spallation Reactions, Neutron Production and Transport
in Thick Lead Target and Uranium Blanket
Irradiated with 0.7 GeV Protons

Neutron activation detectors were used to study a neutron field in setup «Energy plus Transmutation» consisting of thick lead target and natural uranium blanket. This setup was exposed to 0.7 GeV proton beam from the Nuclotron accelerator. The experiment was a part of the systematic study using proton and deuteron beams within the energy range from 0.7 to 2.52 GeV. The experimental data were compared with the results of the MCNPX simulations and with the data of other experiments. Good agreement within the statistical and systematical uncertainties was observed.

The investigation has been performed at the Dzhelepov Laboratory of Nuclear Problems, JINR.

Preprint of the Joint Institute for Nuclear Research. Dubna, 2009

INTRODUCTION

Nowadays there is a strong motivation towards improving precision of predictions of the codes used to simulate production and transport of high-energetic spallation products in material. More realistic simulations will help to design better radiation shielding, more effective spallation neutron sources for condensed matter and material physics, or accelerator-driven subcritical reactors for nuclear waste transmutation. Both thin and thick targets made of different materials were irradiated with relativistic proton beams during various experiments (e.g., [1–3]), which aimed to obtain data about high energy neutron production in spallation reactions.

The international team «Energy plus Transmutation» investigates nuclear processes that occur inside a setup consisting of thick lead target surrounded by a subcritical uranium blanket during irradiations with various proton and deuteron beams (1 GeV protons [4], 1.5 GeV protons [5, 6], 2 GeV protons [7], 1.6 GeV deuterons [8], 2.52 GeV deuterons [9]). All experiments were carried out at the Joint Institute for Nuclear Research (JINR), Dubna, Russia. Within a broad scientific program of the group, the high energy neutron field in this complex setup was studied. The obtained data were used for testing predictions of the computer code MCNPX [10], for total neutron yield simulations, and for tests of high-energy neutron cross sections of selected reactions computed in TALYS [11].

1. EXPERIMENTAL SETUP

The international collaboration «Energy plus Transmutation» designed a setup for the purpose of transmutation studies in high-energy neutron fields (see Fig. 1). It consists of a cylindrical lead target (diameter 84 mm, length 456 mm) and a surrounding subcritical uranium blanket (over 200 kg of natural uranium). The blanket is divided into four sections and each of them contains 30 identical natural uranium rods. These are hermetically encapsulated in an aluminum shell. Each rod has a diameter of 36 mm, a length of 104 mm, and a weight of 1.72 kg.

The blanket is held together by an iron and aluminum construction and is mounted on a wooden plate. Around the blanket, there is a biological shielding consisting of a wooden box with front and back wall opened. One mm thick

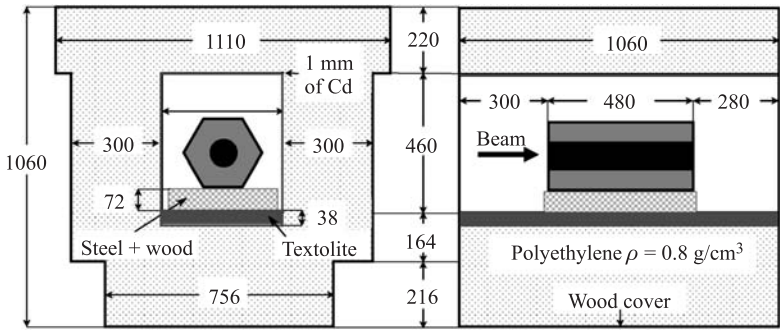

Fig. 1. Cross-sectional front view (left) and side view (right) of the «Energy plus Transmutation» setup. All dimensions are given in millimeters

cadmium plates are mounted on the inner walls of this box, inner volume of the shielding walls is filled with granulated polyethylene. The whole assembly is mounted on an iron stand and it can be moved on rails within the experimental hall. More detailed information about the setup can be found in [12]. Detailed analysis of the influence of different setup parts and uncertainties in their geometrical and physical definitions is examined using the MCNPX code. A similar study was done for possible sources of systematic uncertainties of obtained experimental data, see [13, 14].

2. BEAM MONITORS

Irradiation of the experimental setup was carried out at the Veksler and Baldin Laboratory of High Energy Physics with the 0.7 GeV proton beam extracted from the accelerator Nuclotron. Starting at 17:07 at June 27, 2004, it lasted 32260 s (approximately 9 hours). The exact geometrical adjustment of the experimental setup with respect to the proton beam direction was checked before irradiation by means of sensitive Polaroid film. Because it was very important to know exactly the beam parameters, the proton beam was measured during the irradiation by several groups using different methods. Data from all groups were then used for determination of the beam parameters. The first method applied by Dr. Wagner and his group from Řež was based on activation detectors and it used two sets of Al and Cu square detectors to measure both the intensity and the shape of the beam. The second method was based also on activation detectors, but used Al circular rings placed 57 cm in front of the target to measure the beam intensity and profile at this point. These beam measurements were headed by Dr. Westmeier and Dr. Adam. The third method used by Dr. Zhuk and his colleagues from Belarus was based on solid state nuclear track detectors. Obtained data were used

mainly to verify the beam shape at the beginning of the target and in the first gap of the setup [15, 14]. All experimental results from above-mentioned groups are listed below.

2.1. Square Aluminum and Copper Detectors for Beam Monitoring. Two sets of square aluminum and natural copper (69.17% ^{63}Cu and 30.83% ^{65}Cu) activation detectors were used in this case. Thickness of the foils was 0.1 mm for Al and 0.05 mm for Cu, respectively.

The first set consisted of nine small Cu and Al foils (2×2 cm), was placed directly in front of the target and measured the beam profile and position (Fig. 2). The foils were wrapped up in two layers of paper, stuck as close as possible together, but there were still approximately 3 mm spaces between them (because of double paper wrap).

The second set were big Cu and Al foils (8×8 cm) located in the same place as the circular rings (placement 57 cm in front of the target minimized the activation of the foils by high-energy neutrons emitted backwards from the setup itself). These activation foils measured the total proton fluence on the target.

Gamma radiation of the irradiated monitor foils was measured by two different HPGe detectors at two different geometries (distances 25 and 53 mm from the detectors front). For the gamma measurement, one square sample with the size 2×2 cm (approximate thickness 0.5 mm) was folded from the big beam monitor foil. HPGe detectors were Ortec GMX-20190-P with portable Dewar. Detectors were placed inside lead shielding with the back wall opened. This shielding partially suppressed the background; moreover, it shielded the personnel from measured samples. The detector systems were calibrated using well-defined ^{54}Mn, ^{57}Co, ^{60}Co, ^{88}Y, ^{109}Cd, ^{113}Sn, ^{133}Ba, ^{137}Cs, ^{139}Ce, ^{152}Eu, ^{228}Th, and ^{241}Am point sources which have several gamma lines ranging from 80 to 2615 keV. The calibration gamma spectra were analyzed and net peak areas were calculated using the program DEIMOS [16]. All necessary corrections on possible coincidences and background contributions were made. The systematic uncertainty of the efficiency determination is $\sim 3\%$ for distant geometries and $\sim 6\%$ for the nearest geometry. After all measurements, the calibration was checked once more to control the calibration stability.

Beam monitor foils were measured several times after the irradiation and the following isotopes were identified: ^{56}Co, ^{57}Co, ^{58}Co, ^{52}Mn, ^{54}Mn, ^{51}Cr, ^{48}V, ^{44m}Sc, ^{46}Sc, ^{47}Sc, ^{22}Na, ^{24}Na, and ^{7}Be. The results of the analysis of several γ lines from all spectra were used to calculate the experimental integral proton fluence I_p. Weighted averages over the number of spectra and lines were determined for each individual isotope. The cross sections for different isotope production were obtained from analysis of experimental data from the EXFOR data base [17].

Results of the measurements for different isotopes and at different detector geometries agree within statistical errors and no systematic discrepancies are

visible. The number of used gamma lines $N_{\rm GL}$ and the number of obtained data $N_{\rm D}$ (from repeated measurements at the same or different geometries) for different isotopes are shown in Table 1. The mean weighted average value of the integral proton fluency through the big 8×8 cm monitor placed 57 cm in

Table 1. Proton fluences on the big Cu and Al monitor placed 57 cm in front of the target. Statistical uncertainty includes only uncertainties from the Gauss fit of the gamma peaks in Deimos, in the whole uncertainty is included also uncertainty from cross section

Isotope	σ, mbarn	$\Delta\sigma/\sigma$, %	$N_{\rm GL}$	$N_{\rm D}$	I_p (statistical uncertainty), 10^{13}	I_p (whole uncertainty), 10^{13}
^{56}Co	10.2	7	3	3	1.21(4)	1.21(12)
^{57}Co	26.4	7	2	2	1.40(2)	1.40(12)
^{58}Co	30.0	15	1	1	1.70(3)	1.70(28)
^{52}Mn	9.9	8	3	5	0.99(1)	0.99(9)
^{54}Mn	18.8	6	1	1	1.25(5)	1.25(12)
^{51}Cr	26.7	7	1	1	1.02(4)	1.02(11)
^{48}V	11.5	5	3	3	1.18(2)	1.18(8)
^{44m}Sc	4.00	7	1	2	1.43(3)	1.43(13)
^{46}Sc	5.28	6	1	1	1.25(5)	1.25(12)
^{47}Sc	2.25	7	1	2	1.40(5)	1.40(15)
^{24}Na	10.42	5	2	2	1.20(2)	1.20(8)
^{22}Na	13.8	7	1	1	1.62(21)	1.62(32)
^{7}Be	10.4	5	1	1	1.10(14)	1.10(23)
Weighted average of proton beam intensity						**1.22(5)**
χ^2						1.6

Table 2. Relative proton fluences on nine small monitors placed just in front of the target

Foil number	$N_{\rm D}$	χ^2	Ratio I_p (foil)/I_p (central foil), %
1	25	1.0	62.3(6)
2	24	0.4	88.7(7)
3	24	2.1	49.7(12)
4	25	1.0	73.9(7)
5	24	1.4	100.0(13)
6	24	1.8	66.2(13)
7	21	1.4	43.7(10)
8	19	1.8	62.0(14)
9	19	3.5	39.9(18)

front of the target was determined to be $1.22(5) \cdot 10^{13}$ protons, with the value of $\chi^2 = 1.6$.

To calculate the beam profile and its displacement two assumptions (simplifications) were used — the beam profile is of a circular shape and the proton distribution inside the profile has Gaussian shape. Placement precision for the set of 9 small (2×2 cm) foils was around 2 mm, distances between the foil centers were 2.3 cm. Gamma lines of 13 isotopes (^{56}Co, ^{57}Co, ^{58}Co, ^{52}Mn, ^{54}Mn, ^{51}Cr, ^{48}V, ^{44m}Sc, ^{46}Sc, ^{47}Sc, ^{7}Be, ^{22}Na, and ^{24}Na) produced by high-energy protons in Cu and Al foils were analyzed. The values for production of ^{24}Na on Al foils were influenced by the (n, α) reaction induced by neutrons from the spallation target.

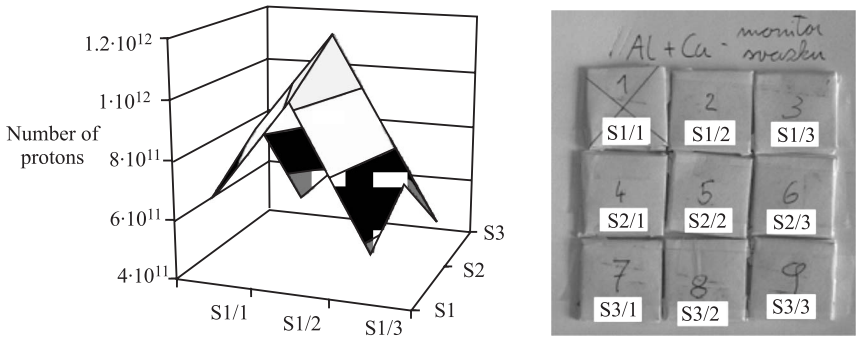

Fig. 2. 3D visualization of the experimental beam profile values measured by the nine small Cu and Al monitors (left) and a photo of real monitors (right)

From this beam determination a shift of the beam 0.5(3) cm upwards and 0.1(3) cm to the left was observed. The total proton fluence via all nine small beam monitors placed directly in front of the target was $0.90(5) \cdot 10^{13}$.

2.2. Aluminum Circular Detectors for Beam Monitoring. Concerning the beam profile at 57 cm in front of the target, the circular rings were used and evaluated in the same way as square monitors. The total ^{24}Na activities of single circular rings are listed in Table 3. The total fluence on the whole 16 cm diameter monitor was $1.40(10) \cdot 10^{13}$ protons. We used these data to obtain the beam profile at a distance of 57 cm by fitting the beam profile by Gaussian distribution. We assumed that the shift of the beam centroid from the center of the monitor was negligible. The fit accuracy can be seen from Table 3 where experimental and fitted data are compared. The systematic uncertainties were deduced from uncertainties of foil positioning, shift of the beam, differences from the circular shape of the beam, and mainly by the non-Gaussian beam tail. The estimate of the variance (σ) uncertainty (from the Gauss fit) is ± 0.3 cm that means $\sigma = 2.7(3)$ cm and FWHM = 6.2(7) cm. Using the obtained beam profile,

Table 3. Data from the big segmented aluminum beam monitor placed 57 cm in front of the target

Foil	Inner diameter, cm	Outer diameter, cm	^{24}Na activity, Bq	Gaussian fit, Bq
Inner circle	0	2.1	21.1(10)	23.7
1$^{\mathrm{st}}$ ring	2.1	8.0	190(13)	190
2$^{\mathrm{nd}}$ ring	8.0	12.0	82(5)	76
3$^{\mathrm{rd}}$ ring	12.0	16.0	19.7(12)	20.7

fluency at this distance from the target was for diameter 8.4 cm (diameter of the lead target) $0.95(6) \cdot 10^{13}$ protons and around 30% of the beam was out of the lead target.

The beam profile results and the data from big square beam monitor (mentioned in Subsec. 2.1) were used to calculate the integral proton fluence at the point 57 cm in front of the target — $1.62(13) \cdot 10^{13}$. The calculated ratio between the whole integral proton flux and the proton flux on the big square monitor is 1.33(12).

2.3. SSNTD Beam Monitoring. The determination of the beam profile using Solid State Nuclear Track Detectors (SSNTD) was realized by the measurement of distributions of induced fission rates in natural lead. Two sets of 37 lead samples were attached in front of the target in two directions: horizontal from

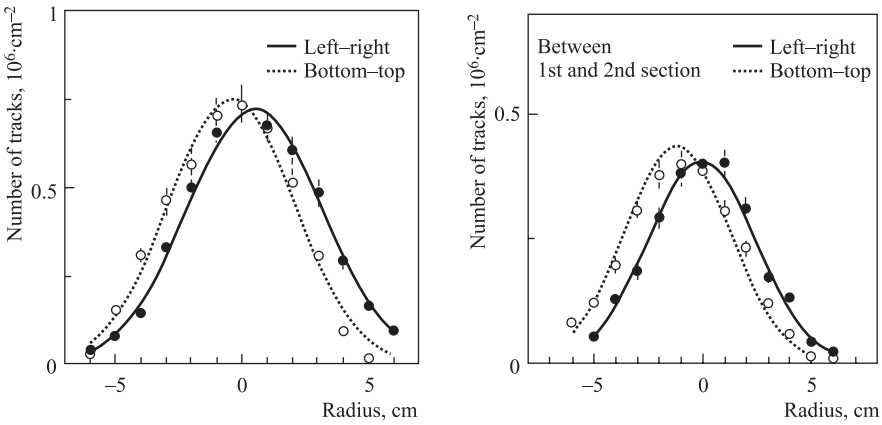

Fig. 3. The Gaussian fits of the beam profile determined by SSNTD. Left: In front of the target: horizontal shift 0.5(3) cm to the right — $\sigma = 2.7(2)$ cm; vertical shift 0.4(3) cm down — $\sigma = 2.5(2)$ cm. Right: In the first gap between the first and the second section: horizontal shift 0.0(3) cm to the right – $\sigma = 2.5(2)$ cm; vertical shift 1.2(3) cm down – $\sigma = 2.4(2)$ cm

left to right side and vertical from bottom to top. Identical sets were also placed between the first and the second sections. Assuming the Gaussian shape of beam profile, following position and profile of the beam were obtained, see Fig. 3.

When we used the beam profile measured by SSNTD and the proton intensity measured by the nine small beam monitors, we got the total proton flux at the point of the target equal to $1.52(15) \cdot 10^{13}$.

2.4. Proton Beam Summary. From SSNTD being the most accurate method for the beam shift monitoring it was assessed that at the beginning of target the beam was shifted 0.4(3) cm downwards and 0.5(3) cm to the right. Results of all beam shift measurements agreed within uncertainties and the beam was within the uncertainties centred to the target axis. Parameters of the Gauss curve at the beginning of the target were $\sigma = 2.51(9)$ cm and FWHM = 5.91(21) cm (good agreement with the distribution obtained with the segmented circular monitors, see Subsec. 2.2). All beam profile measurements showed serious beam divergence and that a certain part of the beam was out of the lead target. Using three different detectors, we measured following proton flux results: $1.52(15) \cdot 10^{13}$ from the nine small monitors placed directly in front of the target, from the segmented circular beam monitors $1.40(10) \cdot 10^{13}$, and $1.62(13) \cdot 10^{13}$ from the big square monitor. Weighted average over these values is equal to $1.49(7) \cdot 10^{13}$ with $\chi^2 = 0.9$. The cross-section uncertainties are included in all quoted uncertainties.

The value $1.52(15) \cdot 10^{13}$ was chosen for further experiment evaluation. Reasons for choosing this value were the following: this value was determined at the beginning of the target from 13 different nuclear reactions (the value $1.40(10) \cdot 10^{13}$ was determined only from one reaction), it was measured at the beginning of the target with the best knowledge about the beam shape measured by SSNTD, and the beam intensity $1.52(15) \cdot 10^{13}$ is close to the weighted average over all beam intensity values, and finally, its uncertainty covers the whole interval of beam results interval.

3. HIGH-ENERGY NEUTRON FIELD MEASUREMENTS

To measure the high-energy neutron field in the «Energy plus Transmutation» setup activation samples were used. On irradiated samples, we looked for products of threshold reactions. Activation samples were foils made of aluminum, cobalt, gold, bismuth, and yttrium. These elements were chosen, because they are either naturally mono-isotopic or one of the isotopes is dominant. They are also cheap, relatively nontoxic, and have convenient physical properties such as melting point or ductility. Further important criteria for choosing these elements were the decay times of isotopes produced through threshold reactions. For more details see Tables 6–10.

High-energy neutrons in the setup emerged mainly from spallation reactions in the lead target. High energy fission in the uranium blanket added some extra neutrons, but there was also an absorption peak on ^{238}U for neutrons around 10 eV (these physical effects were confirmed in MCNPX simulations, see Fig. 14). Furthermore, there was a significant contribution to the epithermal and resonance neutron flux from those neutrons that were moderated in the biological polyethylene shielding and reflected back into the setup. These neutrons created inside the setup a nearly homogeneous field, contrary to spallation neutrons. Nevertheless, we examined the threshold reactions with threshold energies over 5 MeV, which were not affected by these epithermal and resonance neutrons. Only yields of nonthreshold reactions (n, γ) were strongly influenced. This complicated neutron field induced in our activation sensors a lot of various nuclear reactions, mainly of (n, γ), (n, α), (n, p), and (n, xn) type, where the x stands for number of emitted neutrons. Production yields were measured via the characteristic γ-ray spectrum emitted by the products during decay.

Activation samples had a square shape with the length of the side 20 mm (Au and Al samples) or 25 mm (Bi samples), circular shape with diameter of 10 mm (Co samples) or small nuggets (yttrium). The sample placement is depicted in Fig. 4 and listed in Table 4.

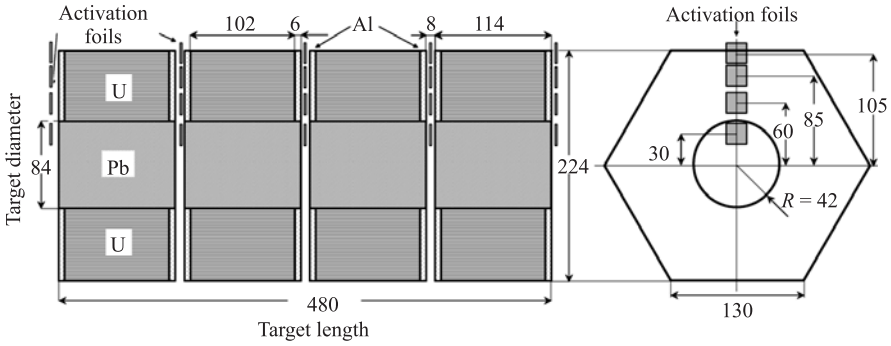

Fig. 4. Placement of the gold and aluminum activation foils. Other elements were placed in similar way, but in another direction from target center to blanket periphery (e.g., bismuth in the right-down direction with respect to the target axis). Dimensions are given in millimeters

Average weight of the foils was 0.3 g for Au, 0.6 g for Al, 2.5 g for Co, 6.5 g for Bi, and 1.1 g for Y. The foils were wrapped in two layers of paper during the irradiation. The inner paper minimized the transport of fission products and produced isotopes out of the foil and also between different foils; moreover, the

Table 4. Placement of activation foils in the «Energy plus Transmutation» setup during 0.7 GeV proton experiment

	Distance from the target axis, cm	Foil label				
1 plane	0					Y1_0
	3	Al1	Au1	Bi1		Y1_1
	6	Al2	Au2			
	8.5	Al3	Au3			
	10.5	Al4	Au4			
2 plane	3	Al5	Au5	Bi2	Co2C1	Y2_1
	6	Al6, Al21, Al22, Al23	Au6, Au21, Au22, Au23	Bi3		Y2_2
	8.5	Al7	Au7	Bi4	Co2C2	Y2_3
	10.5	Al8	Au8	Bi5	Co2C4	Y3_2
	13.5					Y2_0
3 plane	3	Al9	Au9	Bi6		Y3_1
	6	Al10	Au10			
	8.5	Al11	Au11			
	10.5	Al12	Au12			
4 plane	3	Al13	Au13	Bi7		Y4_1
	6	Al14	Au14			
	8.5	Al15	Au15	Bi8		
	10.5	Al16	Au16			
5 plane	0					Y3_0
	3	Al17	Au17	Bi9	Co2_C3	Y5_1
	6	Al18	Au18			
	8.5	Al19	Au19	Bi10		
	10.5	Al20	Au20			

HPGe detector contamination was excluded. The outer paper (removed after the irradiation) minimized contamination of the samples by radioisotopes recoiling from the setup.

Placing the foils closely together had no influence on the yields of threshold reactions (as proven in simulations and published in [13]). Only the yields of nonthreshold (n, γ) reactions were lowered due to self-shielding. Low-energy neutrons were strongly captured due to resonance absorption (e.g., 50% lower yields of (n, γ) ^{198}Au reaction at 50 μm thick gold foil).

Another set of samples was placed on the top of the uranium blanket. It consisted of 10 pairs of gold and aluminum foils mounted horizontally on the blanket construction.

3.1. Evaluation of Reaction Yields in High-Energy Neutron Detectors. After the irradiation, activated high-energy neutron detectors were transported to the spectroscopic laboratory at JASNAPP in order to measure their gamma activities with HPGe detectors (the same detectors as for beam monitors). Almost all samples were measured twice in real time mode. The first measurement was carried out a few hours after the irradiation and lasted only a few minutes, the second one was performed several days up to a few weeks after the irradiation. In that way most produced isotopes except very short-lived ones could be quantified. There was a three-hour gap between the end of the irradiation and the start of the measurement, in which decay of high radioactive contamination of the setup had to be awaited (before this we were not allowed to manipulate with the setup and our samples). This is the reason for not observing isotopes with a half-life shorter than approximately one hour.

To analyze gamma-ray spectra and to determine net peak areas, the computer program DEIMOS [16] was used. Corrections for decay, gamma-line intensity, possible coincidence effects (coincidence summing and background contribution), detector efficiency, beam instability, nonpoint-like emitters, self-absorption and dead-time correction were applied to obtain the total number of nuclei (yield) of certain isotope. This yield was then normalized to 1 g of activation foil and to 1 primary proton (proton beam intensity of $1.52(15) \cdot 10^{13}$ was used). Subsequently one can compare results with other «Energy plus Transmutation» experiments. The final formula for yield calculation is shown below.

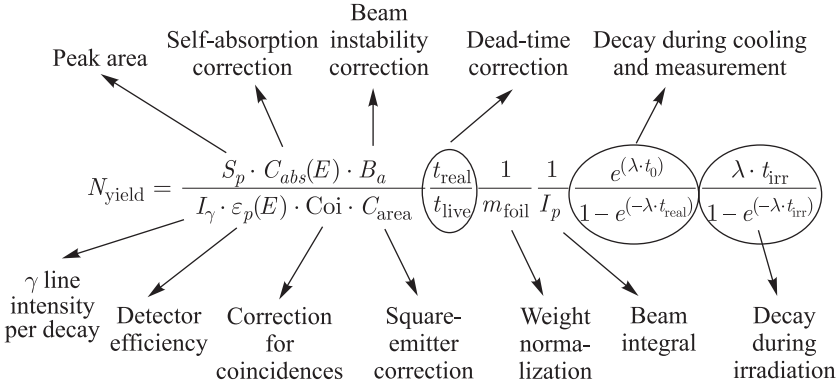

where λ — decay constant, t_{irr} — irradiation time, t_{real} — real measurement time, t_{live} — live time of the detector, t_0 — cooling time.

3.2. Correction on Course of Irradiation. As can be seen from Fig. 5, the beam intensity was not stable during the irradiation and these irradiation instabilities had to be corrected (they have an influence on the yields of observed radioisotopes). We used a program developed in Dubna [18], which counts production and decay of each isotope for each beam bunch, and as an output returns a dimensionless correction factor B_a.

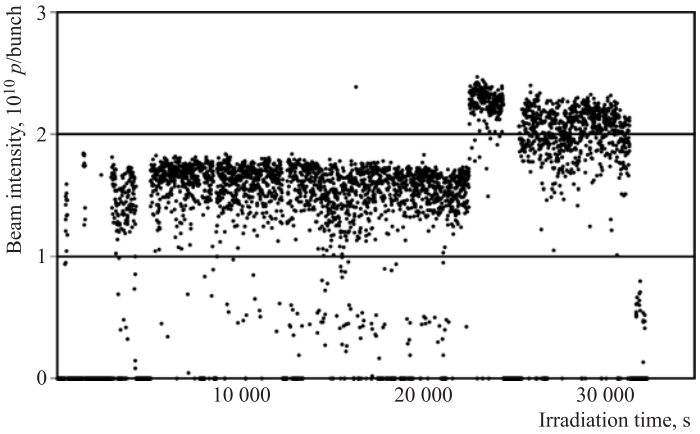

Fig. 5. Beam intensity during the 0.7 GeV proton irradiation of the «Energy plus Transmutation» setup at the Nuclotron accelerator

A less accurate correction factor B_a was obtained by a manual calculation (see Eq. (2)), when the irradiation process was divided into N intervals with constant beam intensity (results from the manual calculation and from the program differs on the second or third decimal place according to the number of intervals). The correction factor generally depends on the half-life of the isotopes, where for short half-life and big changes of the beam at the end of irradiation there are big corrections.

$$B_a = \frac{1 - \mathrm{e}^{-\lambda t_{\mathrm{irr}}}}{t_{\mathrm{irr}} \sum\limits_{i=1}^{N} \left[\dfrac{1}{t_p(i)} W(i)\, \mathrm{e}^{-\lambda t_e(i)} \left(1 - \mathrm{e}^{-\lambda t_p(i)}\right) \right]}, \tag{2}$$

t_{irr} — the total irradiation time; $t_e(i)$ — time from the end of the irradiation interval till the end of the whole irradiation; $t_p(i)$ — time of calculated irradiation interval; $W(i)$ — ratio between the number of protons in the interval and in the whole irradiation; N — the total number of intervals; λ — decay constant.

The beam correction factors for most of the isotopes were very close to unity, only the cases where beam correction factor had influence larger than 2%

Table 5. Beam correction factor B_a for different isotopes calculated by the Dubna program [18]

Isotope	$T_{1/2}$, h	Correction factor, B_a	Isotope	$T_{1/2}$, h	Correction factor, B_a
^{192}Au	4.94	0.972	^{90m}Y	3.16	0.966
^{202}Bi	1.72	0.971	^{85}Y	2.68	0.965
^{201}Bi	1.8	0.970	^{85m}Y	4.86	0.972
^{81}Rb	4.58	0.971	^{82m}Rb	6.47	0.977
Note: Radioisotopes ^{82m}Rb and ^{81}Rb are reaction products from ^{89}Y.					

are shown in Table 5. Beam correction factor was finally checked in a program similar to the program from Dubna, but written in Řež in C++. As both programs use the same analytical method for correction calculations, we get the same results.

3.3. Correction on Nonpoint-Like Emitters. Monte-Carlo simulation was used to assess the effect of nonpoint-like emitters. All detectors were calibrated using standard point-like laboratory etalons, but measured foils had dimensions of 2×2 cm or more. In the simulation the response of the detector on both types of emitters was computed and a ratio square to point-like source (= correction factor) was worked out for the total detector efficiency ε_t (probability of registration of any part of emitted gamma-quantum) and the peak detector efficiency ε_p (probability of registration of whole gamma-quantum written down to the peak of full absorption). Example of the results for 2×2 cm emitter can be seen in Fig. 6.

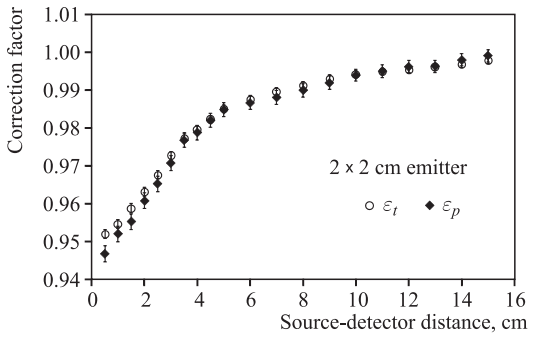

Fig. 6. Correction factor of the total detector efficiency ε_t and the peak efficiency ε_p, nonpoint-like emitter of 2×2 cm size; MCNPX simulation

4. EXPERIMENTAL RESULTS

High-energy neutron spectrum was inspected by means of threshold (n, α), (n, p), and (n, xn) reactions in the detectors. Products with threshold energies E_{thresh} from 5 to 60 MeV were observed, what corresponds to neutron removal multiplicities x from 2 to 9. The values of reaction E_{thresh} were taken from [19], and for higher threshold energies subtracting of the masses of incoming and outgoing particles were used (nuclear masses taken from [20]). Half-lives of isotopes and gamma-line energies were taken from [21]. The yields of observed isotopes (i.e., the numbers of activated nuclei per one gram of the foil and one proton) are shown in the semi-logarithmic scale in Figs. 7–10, corresponding values with uncertainties are given in Tables 6–10. These values represent weighted averages from multiple measurements on various detectors; the uncertainties are only of

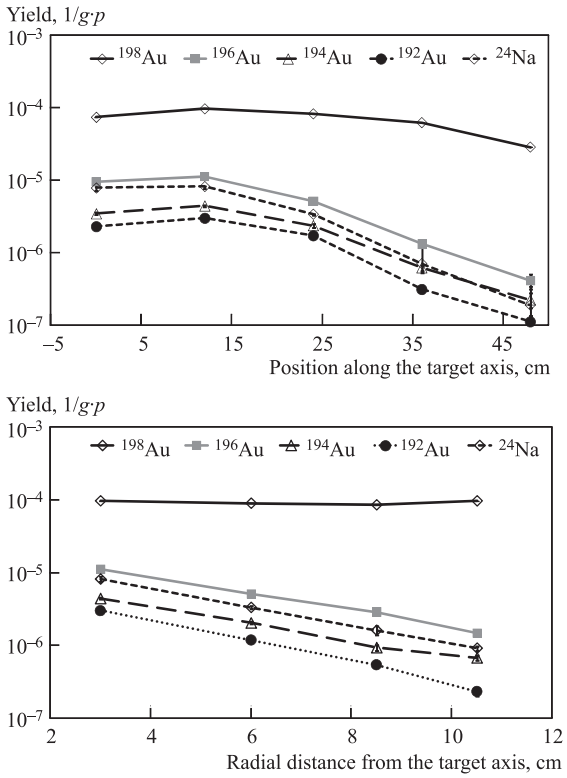

Fig. 7. Yields of observed isotopes in gold and aluminum foils — longitudinal direction 3 cm above the target axis (top) and in radial direction in the first gap of the setup (bottom)

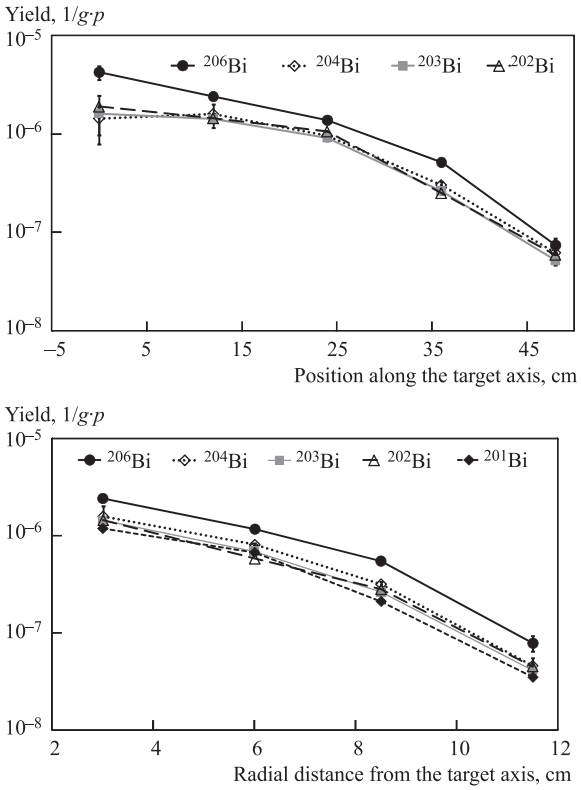

Fig. 8. Yields of observed isotopes in bismuth foils — longitudinal direction 3 cm above the target axis (top) and in radial direction in the first gap of the setup (bottom)

statistical origin from peak fit in DEIMOS32, multiplied by χ^2 for those with χ^2 higher than one.

Products of (p, pxn) reactions leading to the same radioisotope as the (n, xn) reaction cannot be distinguished in the experiment. This can be done only in simulation. From our MCNPX simulations we know that protons can produce up to 20% of the total yield, influence of photons and pions is much smaller (around 1%). When comparing experimental data with the simulated ones, all mentioned reactions are taken into account, see Sec. 5. Experimental points in the following figures are connected with lines to guide reader's eyes. The uncertainties are hardly visible in semi-logarithmical scale.

In Figs. 7–9 the experimental yields are shown as a function of longitudinal and radial coordinates. Basic trends are comparable to the tendencies obtained

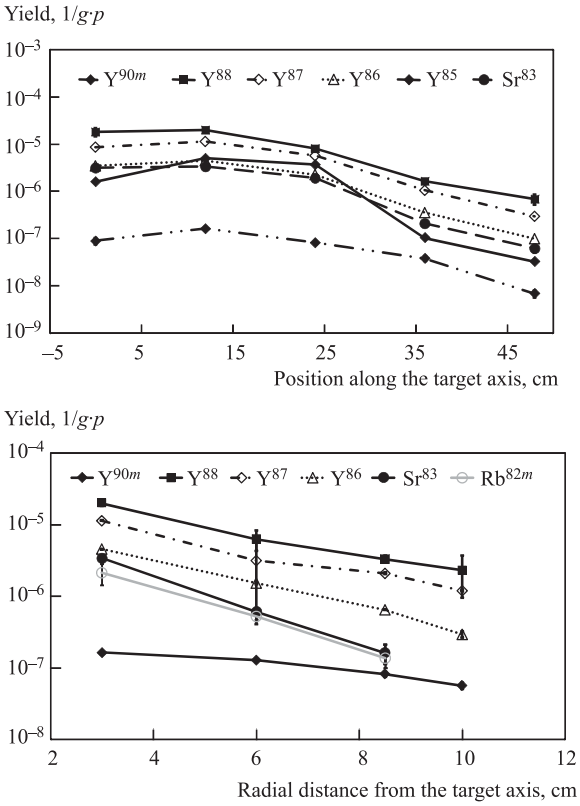

Fig. 9. Yields of observed isotopes in yttrium foils — longitudinal direction 3 cm above the target axis (top) and in radial direction in the first gap of the setup (bottom)

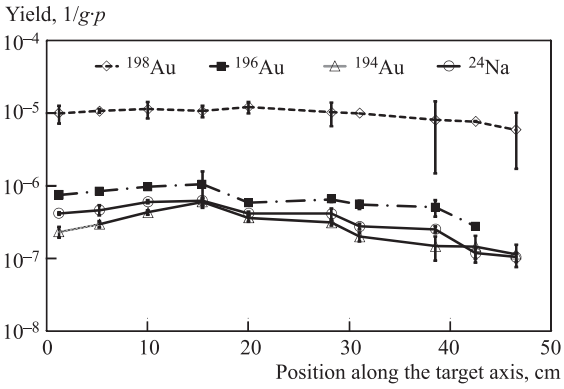

Fig. 10. Yields of observed isotopes in gold and aluminum foils placed on the top the setup in horizontal position. Yields of ^{198}Au are divided by 10

for higher beam energies. Most longitudinal distributions increase slightly until reaching a maximum at around 12 cm from the beginning of the target. Then the longitudinal distributions show a steady decline. The position of the maximum depends on combination of several phenomena, e.g., the angular distribution of particles in spallation reaction, decrease of the proton beam intensity in the target, decrease of primary proton beam energy due to ionization losses of charged particles in material, behavior of a reaction cross section as a function of energy, etc. Neutral particles do not lose energy by ionization; hence the spallation reactions at the end of the target were predominantly induced by secondary high-energy neutrons. It is also visible that ^{198}Au nuclei produced by (n,γ) reactions with thermal neutrons do not have any maximum of yield, as the thermal neutron density distribution from back-diffusion is expected to be flat. The biological shielding really creates an almost homogeneous field of epithermal and resonance neutrons in the target volume.

In the radial direction, yields distribution of all isotopes produced in threshold reactions follow similar trends — a rapid fall with increasing radial coordinate. Such a behavior agrees with the expectation (and we observed it in the previous experiments) that the intensity of the high energetic part of neutron flux drops almost exponentially with growing distance from the spallation source. On

Table 6. Yields of observed isotopes in Bi foils

Foil	^{209}Bi			
Reaction	$(n,4n)$	$(n,6n)$	$(n,7n)$	$(n,8n)$
Product	^{206}Bi	^{204}Bi	^{203}Bi	^{202}Bi
E_{thresh}, MeV	22	38	45	53
$T_{1/2}$, h	150	11	12	2
X, cm	Longitudinal yields for $R = 3.0$ cm, $10^{-6} \cdot \mathrm{g}^{-1} \cdot \mathrm{proton}^{-1}$			
0.0	6(1)	2.1(7)	2.4(12)	2.79(13)
11.8	2.43(16)	1.6(4)	1.44(10)	1.45(7)
24.0	1.39(10)	0.96(7)	0.92(7)	1.064(28)
36.2	0.0359(28)	—	—	—
48.4	0.110(18)	0.092(6)	0.077(8)	0.087(11)
R, cm	Radial yields for $X = 11.8$ cm, $10^{-6} \cdot \mathrm{g}^{-1} \cdot \mathrm{proton}^{-1}$			
3.0	2.43(16)	1.6(4)	1.44(10)	1.45(7)
6.0	1.72(11)	1.20(4)	1.02(6)	0.86(3)
8.5	0.81(4)	0.468(28)	0.390(23)	0.41(10)
10.5	0.116(21)	0.068(14)	0.061(8)	0.066(5)

the other hand, it can be seen that radial distributions change only slightly for isotopes produced in (n,γ) reactions — ^{198}Au. In the radial direction, the biological shielding also creates inside itself almost homogeneous field of epithermal

Table 7. Yields of observed isotopes in Al and Au foils

Foil	^{27}Al	^{197}Au				
Reaction	(n,α)	(n,γ)	$(n,2n)$	$(n,4n)$	$(n,5n)$	$(n,6n)$
Product	^{24}Na	^{198}Au	^{196}Au	^{194}Au	^{193}Au	^{192}Au
E_{thresh}, MeV	5.5	—	8.1	23	30	39
$T_{1/2}$, h	15	65	148	38	18	5
X, cm	Longitudinal yields for $R = 3.0$ cm, $10^{-6} \cdot \mathrm{g}^{-1} \cdot \mathrm{proton}^{-1}$					
0.0	7.9(7)	74(5)	9.6(4)	3.48(14)	11.9(7)	2.33(15)
11.8	8.3(7)	97(27)	11.2(8)	4.46(15)	9.1(8)	3.03(20)
24.0	3.43(15)	83(10)	5.17(14)	2.4(7)	4(4)	1.75(12)
36.2	0.71(18)	63(1.0)	1.31(4)	0.62(14)	1.0(3)	0.32(4)
48.4	0.19(6)	29(9)	0.4(1)	0.23(5)	0.45(15)	0.113(23)
X, cm	Longitudinal yields for $R = 6.0$ cm, $10^{-6} \cdot \mathrm{g}^{-1} \cdot \mathrm{proton}^{-1}$					
0.0	2.57(23)	68(15)	3.81(13)	0.99(20)	1.4(3)	0.67(7)
11.8	3.35(19)	90.0(12)	5.1(5)	2.06(9)	1.74(28)	1.18(6)
24.0	1.85(4)	80(13)	2.93(10)	1.2(7)	1.77(21)	0.90(8)
36.2	0.807(29)	62(8)	1.28(3)	0.66(17)	1.9(4)	0.48(6)
48.4	0.29(15)	33(5)	0.44(3)	0.24(4)	0.09(8)	0.23(4)
X, cm	Longitudinal yields for $R = 8.5$ cm, $10^{-6} \cdot \mathrm{g}^{-1} \cdot \mathrm{proton}^{-1}$					
0.0	1.2(3)	72(21)	1.97(8)	0.50(6)	0.38(15)	0.226(29)
11.8	1.62(23)	85.5(6)	2.89(11)	0.94(23)	0.57(24)	0.54(4)
24.0	0.98(4)	86(5)	1.50(24)	0.58(14)	0.55(24)	0.27(5)
36.2	0.406(18)	63.1(4)	0.7(3)	0.29(18)	0.12(3)	0.192(25)
48.4	0.136(14)	38.2(3)	0.27(4)	0.118(19)	0.021(14)	0.11(3)
X, cm	Longitudinal yields for $R = 10.7$ cm, $10^{-6} \cdot \mathrm{g}^{-1} \cdot \mathrm{proton}^{-1}$					
0.0	0.706(23)	75(18)	1.18(4)	0.26(5)	0.93(24)	0.111(16)
11.8	0.92(6)	97(7)	1.48(13)	0.7(3)	0.00	0.23(3)
24.0	0.57(5)	99(20)	1.16(15)	0.33(6)	1.1(5)	0.25(3)
36.2	0.28(9)	80.6(7)	0.62(8)	0.18(3)	0.21(8)	0.14(4)
48.4	0.112(10)	48.1(1.7)	0.19(2)	0.091(18)	0.15(7)	0.033(14)

Table 8. Yields of observed isotopes in Co foils

Foil	^{59}Co			
Reaction	(n,γ)	$(n,2n)$	$(n,3n)$	$(n,4n)$
Product	^{60}Co	^{58}Co	^{57}Co	^{56}Co
E_{thresh}, MeV	—	13.3	24.6	41.7
$T_{1/2}$, d	1924	78.8	271.8	77.3
R, cm	Radial yields for $R = 11.2$ cm, $10^{-6} \cdot \mathrm{g}^{-1} \cdot \mathrm{proton}^{-1}$			
3.0	27.4(11)	4.09(11)	2.04(9)	1.45(6)
8.5	31.0(13)	1.03(6)	0.59(7)	0.271(28)
10.5	37.9(16)	0.60(6)	0.31(6)	0.074(22)

Table 9. Yields of observed isotopes in Y samples

Foil	^{89}Y				
Reaction	(n,γ)	$(n,2n)$	$(n,3n)$	$(n,4n)$	$(n,5n)$
Product	^{90m}Y	^{88}Y	^{87}Y	^{86}Y	^{85}Y
E_{thresh}, MeV	0	11.5	20.8	32.7	42.1
$T_{1/2}$, h	3	2568	80	15	3
X, cm	Longitudinal yields for $R = 3.0$ cm, $10^{-6} \cdot \mathrm{g}^{-1} \cdot \mathrm{proton}^{-1}$				
0.0	0.090(14)	19(4)	8.74(23)	3.54(9)	2(2)
11.8	0.16(1)	20(4)	11.07(18)	4.57(9)	5.1(6)
24.0	0.099(7)	8.1(5)	5.77(8)	2.31(5)	3.8(8)
36.2	0.039(5)	1.64(20)	1.058(12)	0.358(19)	0.11(11)
48.4	0.0069(12)	0.69(16)	0.298(11)	0.100(7)	0.033(26)
R, cm	Radial yields for $X = 11.8$ cm, $10^{-6} \cdot \mathrm{g}^{-1} \cdot \mathrm{proton}^{-1}$				
3.0	0.16(1)	20(4)	11.07(18)	4.57(9)	5.1(6)
6.0	0.129(9)	6(2)	3.2(28)	1.54(4)	0.6(5)
8.5	0.083(8)	3.4(4)	2.12(20)	0.652(9)	0.18(9)
10.5	0.057(6)	2.3(14)	1.21(4)	0.297(28)	0.08(13)
13.5	0.033(4)	1.13(20)	0.691(17)	0.177(15)	0.052(8)

and resonance neutrons. Comparison with other «Energy plus Transmutation» experiment at higher proton energy can be found in [4].

The set of Al and Au foils placed horizontally on the top of the setup embodied much bigger statistical uncertainties because of low neutron flux at this

Table 10. Yields of observed isotopes in Au and Al foils placed on top of the setup in horizontal position

Foil	^{27}Al	^{197}Au		
Reaction	(n,α)	(n,γ)	$(n,2n)$	$(n,4n)$
Product	^{24}Na	^{198}Au	^{196}Au	^{194}Au
E_{thresh}, MeV	5.5	—	8.1	23
$T_{1/2}$, h	15	65	148	38
X, cm	Longitudinal yields for $R = 15.0$ cm, $10^{-6} \cdot \mathrm{g}^{-1} \cdot \mathrm{proton}^{-1}$			
1.2	0.421(19)	100(28)	0.76(5)	0.23(4)
5.2	0.47(8)	108(7)	0.85(4)	0.300(29)
10.0	0.609(27)	114(29)	0.972(28)	0.43(24)
15.4	0.63(7)	107(19)	1.1(6)	0.60(8)
20.0	0.420(28)	123(22)	0.59(4)	0.36(4)
28.2	0.42(8)	100(40)	0.66(5)	0.32(3)
31.0	0.280(27)	100.2(4)	0.56(8)	0.202(28)
38.5	0.255(24)	80(70)	0.51(13)	0.15(6)
42.5	0.119(18)	77.2(7)	0.278(17)	0.15(6)
46.5	0.106(16)	60(40)	—	0.12(4)

point and thus lower activation of the foils. At this distance the neutron flux was homogenized and the maximum was not visible. The ^{192}Au isotope was not observed what implicates few neutrons with energies over 39 MeV at this place.

Effect of self-shielding decreases the yields of nonthreshold ^{198}Au by $\sim 30\%$ for 50 μm thick foil. In the MCNPX simulation self-shielding is also included, so the correction in experiment is not necessary. Yields of nonthreshold reactions can be thus used to neutron multiplicity assessment; see Sec. 6.

Longitudinal ratios between yields at the end of the target ($X = 48$ cm) and inside the first gap ($X = 12$ cm) as a function of reaction threshold energy are shown in Fig. 11 (left). These longitudinal ratios are within uncertainties almost constant and they exhibit a large spread, reason for that can be relatively low beam energy (protons of 0.7 GeV are fully stopped in the 48 cm thick lead target). In the radial direction, ratios between yields at $R = 10.7$ cm and $R = 3$ cm are shown in Fig. 11 (right). In contrast to the longitudinal ratios, these ratios decrease with increasing threshold energy. This indicates that the resulting neutron spectrum becomes softer at the top of the target.

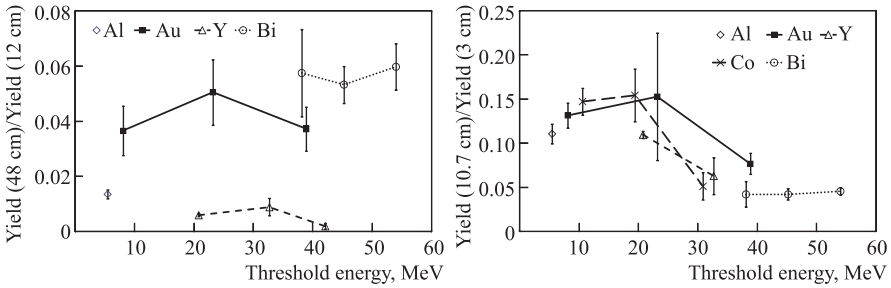

Fig. 11. Ratios of yields at the end of the target ($X = 48$ cm) and inside the first gap ($X = 12$ cm) as a function of threshold energy (left). Ratios of yields at $R = 10.7$ cm and at $R = 3$ cm as a function of threshold energy (right). The lines link points belong to one element

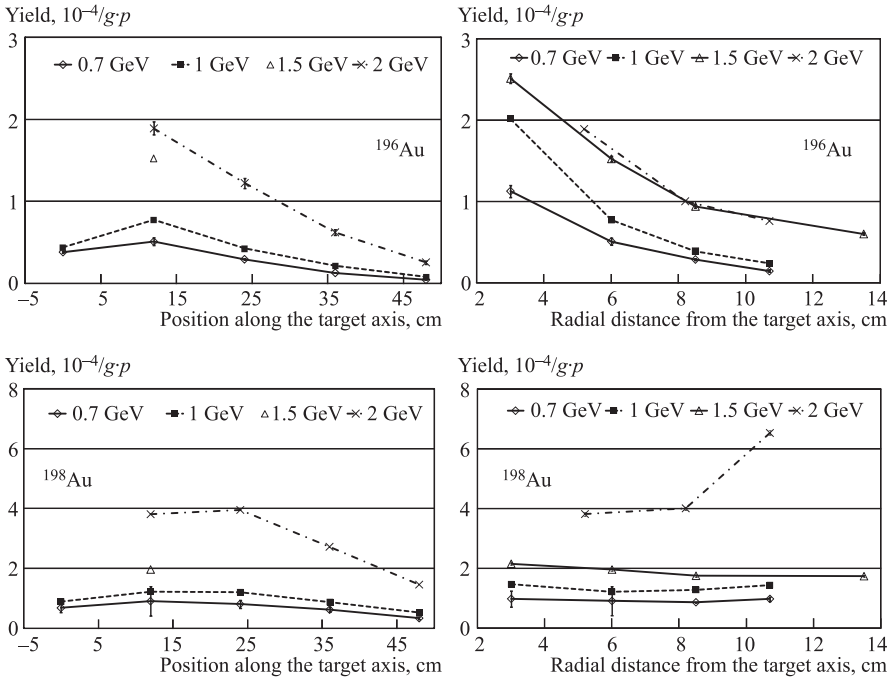

Fig. 12. Comparison among all proton experiments, upper figures for threshold reaction (^{196}Au), lower figures for nonthreshold reaction (^{198}Au). Left figures represent foils placed at distance 6 cm above the target axis, right figures are for the foils in the first gap of the setup

Comparing data from the previous proton experiments on the «Energy plus Transmutation» setup, one can see a clear dependence between the beam energy and density of the neutron flux (all experimental data are normalized to 1 proton). In longitudinal direction, rise of the beam energy causes rising neutron flux and shifting of its maximum farther from the target beginning.

5. COMPARISON WITH MCNPX SIMULATIONS

One of the main aims of this experiment was to compare measured data with simulations. Simulations were performed with the MCNPX 2.6.e code [10]. In the input file, the complex geometry of the uranium rod blanket, the segmented lead target, the polyethylene shielding, all metal frames, shells, and support structures were described; for more details see [13]. The simulated proton beam had energy of 0.7 GeV and a Gaussian profile, its horizontal and vertical FWHM and shift were adjusted to be the same as measured in the experiment (the same amount of protons impinged out of the target in simulation, as in the experiment). Simulations were computed using the intranuclear model INCL4 and the evaporation model ABLA (examples of calculated results are shown in Figs. 16 and 17). This combination of models gives the best agreement with the experiment. Other available combinations of libraries and models were also tested and differences between results up to tens of percents were observed (worse agreement than at INCL4 + ABLA). Detail study of the relation between used models and libraries, and results of the simulations can be found, for example, in [4] (1 GeV proton experiment at «Energy plus Transmutation» setup).

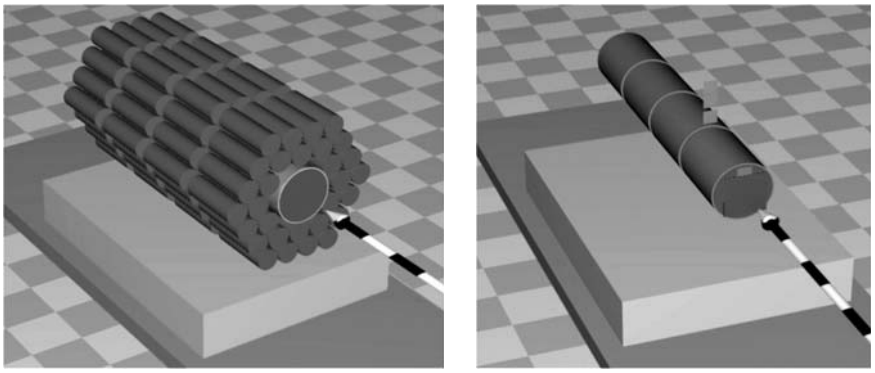

Fig. 13. Model of the «Energy plus Transmutation» setup in MCNPX, rendered in Povray code [22]. The lead target and the uranium blanket without construction materials and shielding are on the left; four sections of the lead target with activation foils are displayed on the right

From the computer simulations significant influence of various parts of the «Energy plus Transmutation» setup onto the neutron field can be seen. In Fig. 14, there is shown a comparison of the neutron spectra in the first part of the target when there were just the lead target (i), or the lead target and construction materials without U and shielding (ii). Then the uranium was added to the target and construction materials (iii), furthermore the biological shielding without cadmium (iiii), and finally a simulation for complete assembly with the biological shielding (iiiii) was performed. From these simulations, it can be concluded that the polyethylene shielding substantially enhances the thermal, epithermal, and resonance component of the neutron flux in the setup. The thermal part of the neutron flux returning to the inner volume of the setup is completely absorbed by the cadmium layer. The shielding box does not significantly change the neutron spectrum above 10^{-2} MeV.

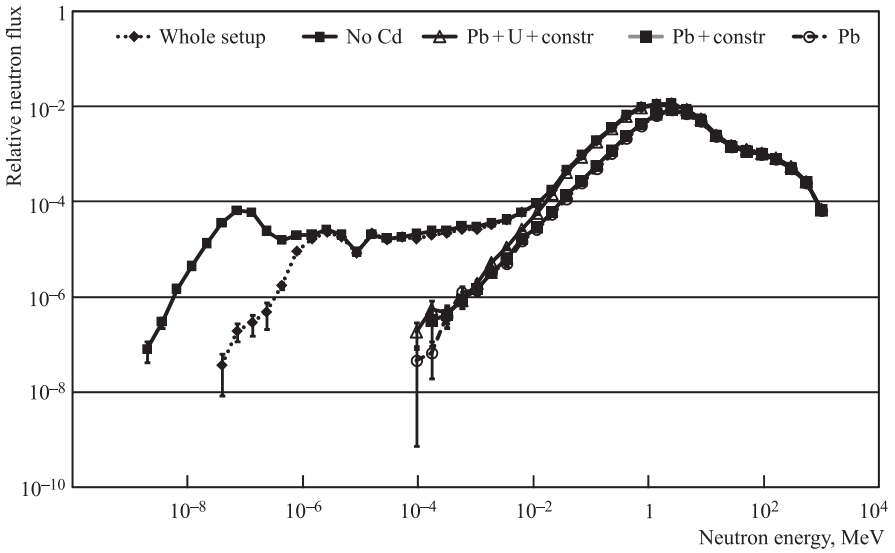

Fig. 14. Setup parts influence on the neutron field in the first target part, MCNPX simulation

The difference between high-energy neutron flux in the bare Pb target and in the Pb target surrounded by the uranium blanket is partly caused by fission of ^{238}U, reflection of high energy neutrons back to the target, and by beam tails, which in the case of the 0.7 GeV proton experiment hit also the uranium blanket, see Fig. 14 (right). MCNPX can calculate directly yields of produced isotopes using the «f4 tally». Unfortunately, cross-section values for threshold reactions at high energies are not very accurate in MCNPX and they can be

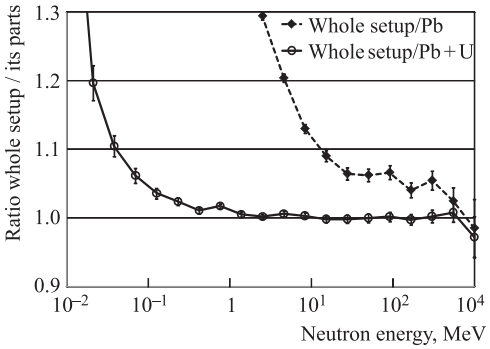

Fig. 15. Ratio in neutron production between the whole setup and the bare lead target, respectively the lead target with uranium blanket; MCNPX simulation

obtained better using the TALYS code ver. 0.79 [11]. Moreover, «f4 tally» cannot calculate the production of radioisotopes through proton and pion induced reactions. Therefore, yields were simulated in MCNPX only of nonthreshold (n,γ) reactions (^{198}Au, ^{209}Bi, etc.) together with secondary neutron, proton, and pion spectra. These spectra were then folded with simulated cross sections computed separately in TALYS for lower energies up to 200 MeV and in MCNPX for higher energies. TALYS and MCNPX cross sections were finally connected together.

The ratios of yields obtained from the experiment and from the MCNPX simulation of the whole setup are plotted in Figs. 16 and 17. Lines between the points are meant to guide reader's eyes. If we watch for the trends in the data, it may be stated that the MCNPX simulation provides qualitatively

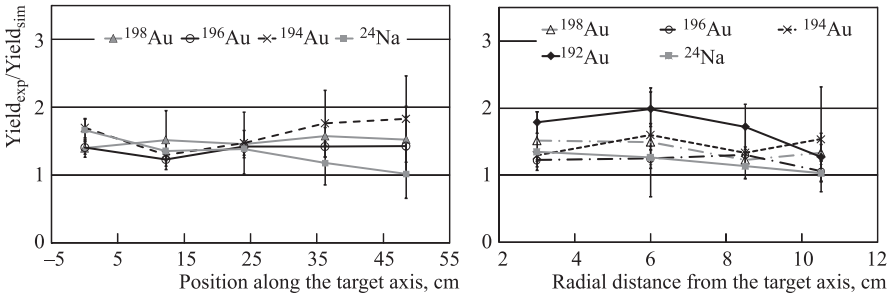

Fig. 16. Experiment versus simulation ratio of Au and Al yields, left — in longitudinal direction 3 cm above the axis, right — in radial direction in the first gap of the «Energy plus Transmutation» setup

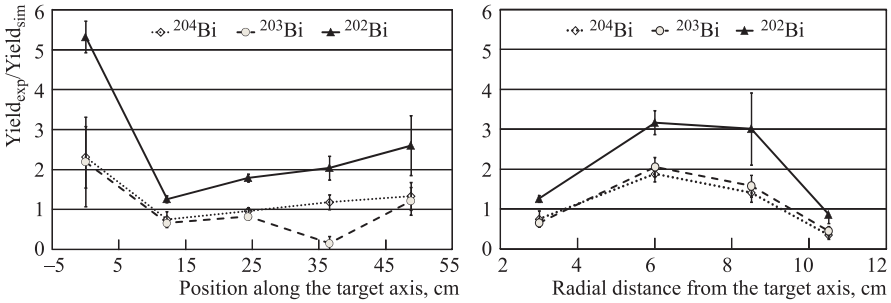

Fig. 17. Experiment versus simulation ratio of Bi yields, left — in longitudinal direction 3 cm above the axis, right — in radial direction in the first gap of the «Energy plus Transmutation» setup

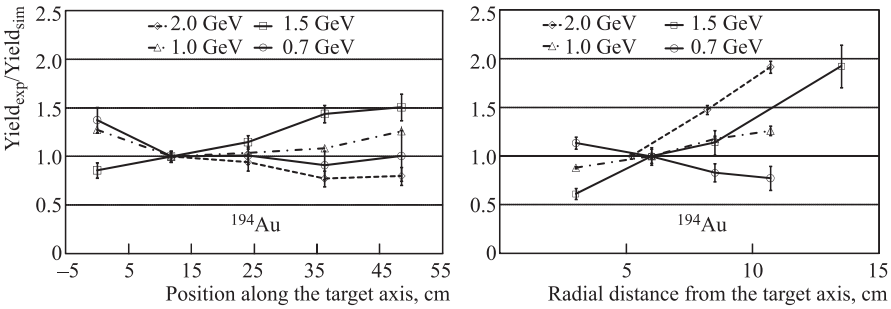

Fig. 18. Comparison of normalized experimental and simulated (Bertini + Dresner) yields of ^{194} Au in longitudinal direction at 6 cm from the target axis (left), and in radial direction in the first gap (right) for all proton experiments. Data are normalized to the second foil in each set

reliable prediction for measured data, especially for Au and Al. Any substantial disagreement in radial direction was not observed, contrary to experiments with proton energy 1.5 GeV (see Fig. 18) and higher.

6. DETERMINATION OF NEUTRON MULTIPLICITY

The so-called water-bath/activation foil method [23] is often used for the determination of the integral numbers of neutrons produced in thick targets. The conventional variant of this method uses two basic premises: neutrons from the source are predominantly contained within the moderator volume; and it is

possible to integrate the measured thermal flux distribution over the water volume with adequate precision. As the latter requires the usage of a large-scale grid of activation foils, we used the new form of this method [1], which replaces the flux integration by relating a small-scale set of foil activities to the integral quantity — the integral number of neutrons produced per one beam particle (so-called neutron multiplicity) $n_{\mathrm{tot}}^{\mathrm{exp}}$ obtained by simulation.

Polyethylene in the «Energy plus Transmutation» setup worked as a water bath — it moderated the outgoing neutrons. The front and back openings of the shielding were neglected. Multiplicity simulations were done in MCNPX 2.6.e using INCL4 + ABLA models (the neutron multiplicity does not depend significantly on the combination of the models available in MCNPX in this energy region). For calculation of the neutron multiplicity, the ratios between experimental and simulated yields of ^{198}Au in all gold samples were determined. The weighted average over these samples was determined and multiplied with the simulated neutron multiplicity

$$n_{\mathrm{tot}}^{\mathrm{exp}} = n_{\mathrm{tot}}^{\mathrm{sim}} \left\langle \frac{N_{\mathrm{yield}}^{\mathrm{exp}}}{N_{\mathrm{yield}}^{\mathrm{sim}}} \right\rangle . \tag{3}$$

The advantage of this procedure is that the experimental value of neutron multiplicity $n_{\mathrm{tot}}^{\mathrm{exp}}$ is highly insensitive to the simulated value $n_{\mathrm{tot}}^{\mathrm{sim}}$ and its uncertainty. Assuming that the MCNPX describe well the spatial distribution of the neutrons as well as the shape of low energy part of neutron spectrum and its approximate magnitude; the product of the two terms in Eq. (3) effectively cancels out the dependence on $n_{\mathrm{tot}}^{\mathrm{sim}}$.

In the case of 0.7 GeV proton «Energy plus Transmutation» experiment the fraction $\left\langle \frac{N_{\mathrm{yield}}^{\mathrm{exp}}}{N_{\mathrm{yield}}^{\mathrm{sim}}} \right\rangle$ is equal to 1.32 ± 0.04, $n_{\mathrm{tot}}^{\mathrm{sim}}$ equals 18.2, and $n_{\mathrm{tot}}^{\mathrm{exp}}$ is equal to 24.0 ± 2.4 neutrons (absolute), i.e., 34.3 ± 3.4 neutrons per GeV. Comparison among all proton and deuteron experiments at «Energy plus Transmutation» setup will be presented in a forthcoming publication related to deuterons.

In the 0.7 GeV proton experiment set of gold foils was placed horizontally on the top of the setup. These foils were placed in the most convenient place for the multiplicity measurements; in the place where the epithermal and resonance neutron field is almost homogeneous and minimally affected by the target and uranium blanket. Neutrons of low energies diffuse back from the biological shielding (production of the ^{198}Au in this place can be seen in Fig. 10). When using the results of these foils to determine neutron multiplication, one gets almost the same results as from the foils placed inside the target-blanket assembly: $\left\langle \frac{N_{\mathrm{yield}}^{\mathrm{exp}}}{N_{\mathrm{yield}}^{\mathrm{sim}}} \right\rangle$ is 1.36 ± 0.04, and $n_{\mathrm{tot}}^{\mathrm{exp}}$ is equal to 24.8 ± 2.5 neutrons (absolute), respectively, 35.4 ± 3.5 neutrons per GeV. This confirms that the multiplication factor can either be calculated from the foils placed inside the target-blanket

assembly without a serious systematic uncertainty. The total uncertainty of the neutron multiplicity includes also the uncertainty from the beam intensity determination.

CONCLUSIONS

The neutron field produced in the experimental setup called «Energy plus Transmutation» was studied by means of activation analysis. The setup consisted of a thick lead target, a natural uranium blanket, and a surrounding polyethylene radiation shielding. The activation detectors were mostly thin foils made of gold, bismuth, aluminum, yttrium, and cobalt. The lead target was irradiated with 0.7 GeV proton beam from the Nuclotron accelerator with a total intensity of $1.52(15) \cdot 10^{13}$ particles. Several systems for beam monitoring were used to measure the beam shape, displacement and total intensity.

The γ-ray spectra of activated detectors were analyzed in order to get the yields of (n, γ), (n, xn), and (n, α) reactions. When evaluating the yields, various spectroscopic corrections were applied to control all possible sources of systematic uncertainties. Finally, the experimental yields of ^{198}Au, ^{196}Au, ^{194}Au,^{192}Au, ^{24}Na, ^{204}Bi,^{203}Bi, and ^{202}Bi isotopes were compared with the results of the MCNPX simulation with a good qualitative agreement. The simulations follow quite well the trends of measured data, where trends are insensitive to beam intensity determination and to absolute values of simulated cross sections. Contrary to trends, absolute values of the exp/sim ratios depend strongly on the beam intensity determination and simulated cross-section values. The ratio exp/sim at threshold reactions is for most of observed isotopes higher than one, which is in agreement with the exp/sim ratio at nonthreshold reactions on gold foils used for neutron multiplicity determination.

A modified method of water bath was used to assess the integral number of neutrons produced at the «Energy plus Transmutation» setup (neutron multiplicity). Using the simulated number of produced neutrons and the above-mentioned ratios exp/sim for ^{198}Au, we determined the neutron multiplicity for 0.7 GeV proton experiment equal to 24.0 ± 2.4, respectively 34.3 ± 3.4 per GeV.

After this proton experiment two more irradiations of the «Energy plus Transmutation» setup with relativistic deuterons were performed and their results will be published soon.

Acknowledgements. The authors thank the LHEP JINR (Dubna) for using the Nuclotron accelerator and to the Agency of Atomic Energy of Russia for supply of material for the uranium blanket. This work was carried out under the support of the Grant Agency of the Czech Republic (grant No. 202/03/H043) and purpose financial support from Academy of Sciences of the Czech Republic (No. K2067107).

REFERENCES

1. *Van der Meer K. et al.* // Nucl. Instr. Meth. Phys. Res. B . 2004. V. 217. P. 202–220.
2. *Majerle M. et al.* // J. Phys Conf. Ser. 2006. V. 41. P. 331–339.
3. *Letourneau A.* // Nucl. Instr. Meth. Phys. Res. B. 2000. V. 170. P. 299–322.
4. *Krása A. et al.* Neutron Emission in the Spallation Reactions of 1 GeV Protons on a Thick Lead Target Surrounded by Uranium Blanket. JINR Preprint E15-2007-81. Dubna, 2007.
5. *Krivopustov M. I. et al.* Investigation of Neutron Spectra and Transmutation of ^{129}I, ^{237}Np and Other Nuclides with 1.5 GeV Protons from the Dubna Nuclotron Using the Electronuclear Setup «Energy plus Transmutation». JINR Preprint E1-2004-79. Dubna, 2004.
6. *Křižek F. et al.* // Czech J. Phys. 2006. V. 56. P. 243.
7. *Krása A. et al.* Neutron Production in $p+\mathrm{Pb/U}$ at 2 GeV. JINR Preprint E1-2009-195. Dubna, 2009.
8. *Krivopustov M. I. et al.* Investigation of Neutron Generation and Transmutation of ^{129}I, ^{237}Np, ^{238}Pu, ^{239}Pu at the Experiment Using the U/Pb Assembly Irradiated with 1.60 GeV Deuterons. JINR Preprint E1-2008-54. Dubna, 2008.
9. *Krivopustov M. I. et al.* About the First Experiment on Investigation of the ^{129}I, ^{237}Np, ^{238}Pu and ^{239}Pu Transmutation at the Nuclotron 2.52 GeV Deuteron Beam in Neutron Field Generated in Pb/U-Assembly «Energy plus Transmutation». JINR Preprint E1-2007-7. Dubna, 2007.
10. MCNPX (Monte Carlo N-Particle code eXtended). http://mcnpx.lanl.gov/ (19.1.2009).
11. *Koning A. J. et al.* // Proc. of the Intern. Conf. on Nuclear Data for Science and Technology — ND2004. V. 769. AIP, 2005.
12. *Krivopustov M. I. et al.* // Kerntechnik. 2003. V. 68. P. 48–55.
13. *Majerle M. et al.* // Nucl. Instr. Meth. Phys. Res. A. 2007. V. 580. P. 110–113.
14. *Majerle M. et al.* Monte Carlo Method in Neutron Activation Analysis. JINR Preprint E11-2009-178. Dubna, 2009.
15. *Zhuk I. V. et al.* // Rad. Meas. 2008. V. 243. S210–S214.
16. *Frána J.* // J. Rad. Nucl. Chem. 2003. V. 257, No. 3. P. 583–587.
17. Experimental Nuclear Reaction Data (EXFOR). http://www-nds.iaea.org/exfor/exfor.htm, (20.3.2009).
18. *Kumawat H.* Development of Cascade Program and Its Applications to Modeling Transport of Particles in Many Component Systems. PhD. Thesis. JINR, Dubna, 2004.
19. Qtool: Calculation of Reaction Q-Values and Thresholds. http://t2.lanl.gov/data/qtool.html, (22.3.2009).
20. Ground State Masses and Deformations. http://t2.lanl.gov/data/astro/molnix96/massd.html, (1.12.2008).

21. *Chu S. Y. F. et al.* The Lund/LBNL Nuclear Data Search web page. http://nucleardata.nuclear.lu.se/nucleardata/toi/ (1.12.2008).

22. POVRAY — The Persistence of Vision Raytracer — High-Quality, Totally Free Tool for Creating Stunning Three-Dimensional Graphics. http://www.povray.org/ (5.12.2008).

23. *Beckurts K. H., Wirtz K.* Neutron Physics. Berlin; Göttingen; Heidelberg; N. Y.: Springer-Verlag, 1964.

Received on November 19, 2009.

Корректор *Т. Е. Попеко*

Подписано в печать 18.03.2010.
Формат 60 × 90/16. Бумага офсетная. Печать офсетная.
Усл. печ. л. 1,93. Уч.-изд. л. 2,63. Тираж 290 экз. Заказ № 56940.

Издательский отдел Объединенного института ядерных исследований
141980, г. Дубна, Московская обл., ул. Жолио-Кюри, 6.
E-mail: publish@jinr.ru
www.jinr.ru/publish/